Journal of Power Sources 196 (2011) 2893–2898

Contents lists available at ScienceDirect

Journal of Power Sources

journal homepage: www.elsevier.com/locate/jpowsour

Comparative study of composite electrodes containing tin, polyacrylonitrile and cobalt or iron

Francisco Nacimiento, Ricardo Alcántara*, José L. Tirado

Laboratorio de Química Inorgánica, Universidad de Córdoba, Edificio C3, Planta 1, Campus de Rabanales, 14071 Córdoba, Spain

ARTICLE INFO

Article history:
Received 30 July 2010
Received in revised form
21 September 2010
Accepted 7 November 2010
Available online 12 November 2010

Keywords:
Lithium ion batteries
Alloys
Intermetallics
Tin
Polyacrylonitrile

ABSTRACT

Composite materials containing Co–Sn alloys and polyacrylonitrile (PAN) have been prepared by reduction of Co(II) and Sn(II) in dimethylformamide with $NaBH_4$. The resulting cobalt and tin form an amorphous alloy and the PAN molecules hinder the growth and crystallization of the metallic grains. After heating the composite material obtained at 300 °C in Ar-atmosphere, the amorphous alloy leads to poorly crystallized $CoSn_2$, and the PAN molecules are partially pyrolyzed. In contrast, the reduction of Fe(II) and Sn(II) leads to crystalline Sn. The electrode containing nanosized $CoSn_2$ and PAN shows an excellent electrochemical behavior in lithium cells due to the structural stability of the PAN matrix and the small size of the metallic grains.

1. Introduction

Tin possesses the chemical property to alloy extensively with lithium. This feature makes tin and tin compounds very promising for lithium ion batteries electrodes. However, pure tin commonly exhibits very rapid capacity fade in a few charge–discharge cycles. Several intermetallic compounds and alloys containing tin and cobalt seem to be particularly useful [1,2]. Thus, CoSn [3], $CoSn_2$ [4,5], Co_3Sn_2 [5–7] and $CoSn_3$ [8] compounds, and Co–Sn–C alloys [2,9] have been studied as electrode materials. It seems that the cobalt atoms stabilize tin-based electrodes upon cycling, by buffering volume changes and avoiding grain growth. The theoretical specific capacity decreases when cobalt is added, as compared with pure tin. The substitution of cobalt by iron can be advantageous from toxicological and economic perspectives. Interestingly, $CoSn_2$ and $FeSn_2$ are isostructural (space group I4/mcm). It has been proposed that the structure of $CoSn_2$ (and $FeSn_2$) has tunnels among the Sn atoms where Li might penetrate to initiate the reaction and, however, neither CoSn nor Co_3Sn_2have such tunnels [1]. Carbon is another relevant component of the tin-based electrodes, which can enhance the connectivity between the metallic particles and stabilize the whole composite electrode [1]. Graphite, disordered carbon or organic polymers may be used as a source of carbon for the tin-based electrode. The use of small particles, amorphous alloys or nanocrystalline compounds is apparently an important prerequisite to achieve excellent electrochemical behavior. The large particles drive to breakage of the grains, swelling of the electrode and electrolyte consumption.

The reaction between lithium and Co–Sn compounds has been the subject of several studies that highlight the influence of grain size on the electrochemical reactions. Fan et al. proposed that amorphous CoSn forms Li–Co–Sn alloys [10]. The reaction between crystalline $CoSn_2$ and Li was studied by Ionica-Bousquet et al. [4]. Recently, Ferguson et al. concluded that fully lithiated $Co_3Sn_3C_4$ prepared by mechanical attrition is composed of nanoscale regions of $Li_{22}Sn_5$, nanoscale Co and lithiated carbon, while CoSn grains form after lithium extraction [11].

Polyacrylonitrile (PAN) is a very versatile polymer of formula $(-[CH_2-CH(CN)]_n-)$, having several applications in the field of batteries. Thus, PAN molecules, together a plasticizer and a lithium salt, can be used to prepare a solid electrolyte for lithium batteries [12]. PAN molecules can also be used as precursor to prepare carbon fibers [13] and hard-carbons [14] that can be used as electrode active materials for lithium ion batteries. After pyrolysis at moderate temperatures [15], PAN molecules can form a conductive matrix of carbon that surrounds Sn particles [16]. PAN molecules have also been used to encapsulate $CoSn_2$nanoparticles, and the TEM images showed that the metallic particles with nanometric size were surrounded by a carbonaceous film [17,18]. The use of PAN to create Si-filled carbon fibers for lithium ion batteries also has been reported [19].

* Corresponding author. Tel.: +34 957218637; fax: +34 957218621.
E-mail address: iq2alror@uco.es (R. Alcántara).

0378-7753/$ – see front matter © 2010 Elsevier B.V. All rights reserved.
doi:10.1016/j.jpowsour.2010.11.034

In this work, a comparative study on the preparation and properties of Co–Sn–PAN and Fe–Sn–PAN composites, and the role that is played by the PAN molecules is carried out. The effect of annealing at 300 °C the PAN-containing electrode materials is also studied.

2. Experimental

For the preparation of Co–Sn–PAN composite, first 4.0 g of $SnCl_2{\cdot}2H_2O$, 2.1 g of $CoCl_6{\cdot}6H_2O$ and 0.6 g of polyacrylonitrile (PAN, with M_W = 150.000) were added into 250 mL of n,n-dimethylformamide (DMF) with continuous stirring. Second, an aqueous solution of $NaBH_4$ was added. Then, further water was added. It is worth noting that PAN is highly soluble in DMF and scarcely soluble in water. The resulting precipitate was separated by centrifugation, rinsed several times and dried under vacuum at 120 °C overnight. For the sake of comparison, a sample was prepared by using an equivalent procedure but without addition of PAN. Alternatively, iron(II) chloride was used instead of cobalt chloride to prepare Fe–Sn–PAN composites. All the reagents were supplied by Aldrich. The Co–Sn–PAN composite sample was further annealed at 300 °C during 3 h under an Ar-flow of 90 mL min^{-1}.

X-ray diffraction patterns were recorded in a Siemens D5000 instrument and using 0.04°-2 s steps. The average grain size was calculated by applying the Scherrer equation ($Lc = 0.9\lambda/\beta\cos\theta$) to the most intense Bragg reflection. Carbon and nitrogen contents were determined in an elemental analyzer Eurovector EA3000. Differential thermal analysis (DTA) experiments were carried out by using a Shimadzu DTG-60 instrument, alumina pans, 10 °C min^{-1} of heating rate and 50 mL min^{-1} of Ar-flow.

To study the pyrolysis of PAN, pure PAN was heated in an alumina crucible under Ar-flow (90 mL min^{-1}) at temperatures between 300 and 600 °C, with a heating rate of 1.5 °C min^{-1} and the imposed temperature was hold during 3 h. The NMR spectra of the resulting residua were recorded. Solid state ^{13}C NMR spectra were recorded in a BrukerAvance 400 WB instrument.

The electrochemical behavior of the prepared materials was studied in lithium test cells. A piece of Li was used as negative electrode. The positive electrode contained active material (70%), carbon black (20%) and polyvinylidene fluoride (PVDF) like binder (10%). A 1 M solution of $LiPF_6$ in an ethylene carbonate:diethyl carbonate solvents mixture (EC:DEC = 50:50) was used as electrolyte. The instrument to carry out the discharge–charge cycling experiments was as a VMP. Typically, a mass-normalized constant current of 50 mA g^{-1} and 0.0–0.9 V of potential window were imposed for the cycling experiments. Experiments were also performed at variable current intensities. Co, Sn and PAN were considered in the calculation of the specific capacity.

3. Results and discussion

The sample obtained by reduction of cobalt and tin ions in DMF without PAN shows a XRD pattern (Fig. 1) with intense Bragg reflections corresponding to well crystallized $CoSn_2$ (main phase) and β-Sn (minor phase). The calculated grain size of $CoSn_2$ is Lc = 36 nm. In contrast, the sample obtained with PAN possesses an amorphous character. The dispersed molecules of PAN do not drive to any XRD diffraction. After annealing this amorphous sample at 300 °C under Ar-flow, a low-intensity reflection emerges which can be ascribed to $CoSn_2$ (ICDD File No. 25-0256), although the possible presence of amorphous alloys cannot be ignored. The calculated grain size value for $CoSn_2$ is Lc = 18 nm. These samples, that contain intermetallic particles surrounded by PAN [17], can be named like $CoSn_2$@PAN. The XRD patterns of the samples obtained by reduction of iron and tin ions in the presence of PAN, or without PAN, show in both cases intense reflections corresponding to crystalline β-Sn with

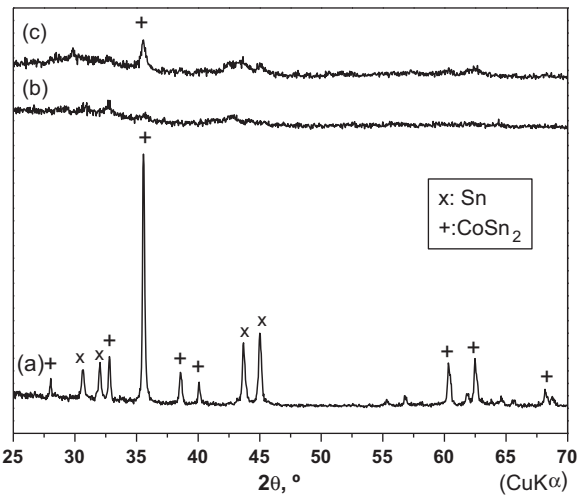

Fig. 1. XRD patterns of (a) $CoSn_2$, (b) $CoSn_2$@PAN and (c) $CoSn_2$@PAN annealed at 300 °C under Ar-flow. The samples corresponding to (a) and (b) were heated up to 120 °C under vacuum.

Lc = 30 nm (Fig. 2). Only traces of $FeSn_2$ are found. These samples, that contain crystalline tin, PAN and iron with no apparent interaction between them, can be named like Fe–Sn–PAN. In principle, it would be easier to reduce Fe(II) ions than Co(II) ions. Nanocrystalline Fe would lead to a low-intensity reflection placed at ca. 44.7°2θ overlapping with Sn reflections. The Fe–Sn–PAN sample showed a strong tendency to react exothermally with the air atmosphere when it was manually ground in an agate mortar, yielding to iron and tin oxides (XRD not shown).

The DTA curve of $CoSn_2$@PAN does not show the endothermal peak corresponding to the melting point of tin. The exothermal peak observed at 295 °C (Fig. 3) may be due to grain growth and crystallization of the amorphous alloy and/or PAN pyrolysis. This peak is not observed after cooling down and recording the DTA curve during a second heating process. The $CoSn_2$ sample obtained without adding PAN does show neither the melting point of tin nor the exothermal peak at 295 °C. In contrast, the DTA curve of the sample prepared with iron instead of cobalt shows an endothermal peak at the melting point of Sn (232 °C) besides endothermal peaks at 115–133 °C due to solvent evaporation (Fig. 4). The melting point of Sn is not observed after cooling the sample and recording the

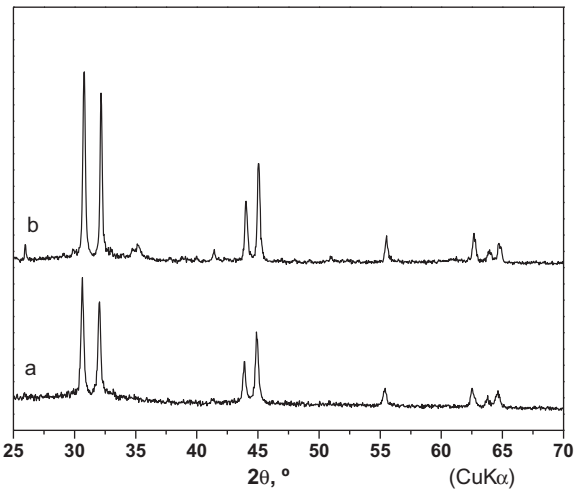

Fig. 2. XRD patterns of (a) Fe–Sn and (b) Fe–Sn–PAN samples heated up to 120 °C under vacuum.

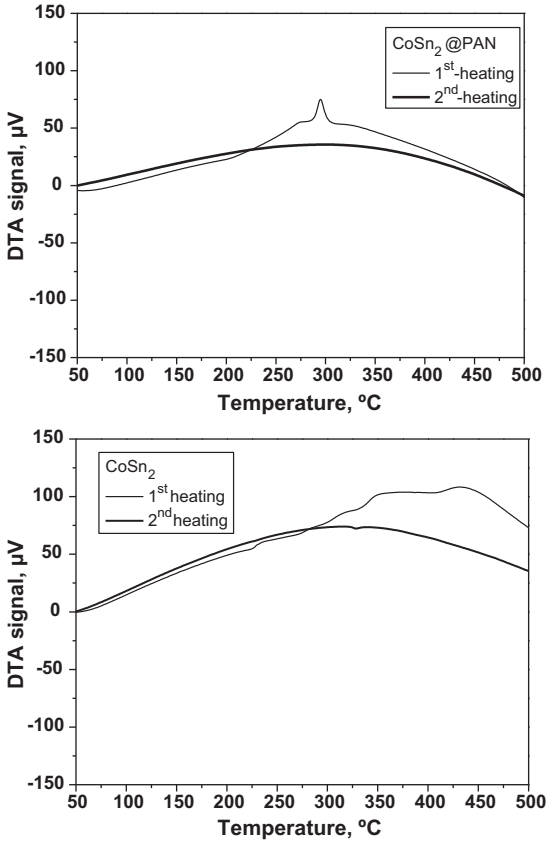

Fig. 3. DTA curves for $CoSn_2$@PAN and $CoSn_2$ prepared without adding PAN.

DTA, suggesting that tin reacts to form other compounds during the first heating.

All these XRD and DTA results evidence the two following features: (i) the easier tin/cobalt diffusion to form alloys and intermetallics in comparison with tin/iron, and (ii) the addition of polymer PAN hinders the grain growth of $CoSn_2$. It is known that cobalt and tin have great ability to form amorphous alloys [20–22].

The experimental contents in carbon and nitrogen for $CoSn_2$@PAN-120 °C are 10.0 and 3.5% by mass, respectively. After annealing at 300 °C, the carbon and nitrogen contents decrease to 8.8 and 2.7%, respectively. These data reflect an incomplete pyrolysis and denitrogenation of the PAN molecules. It is expected

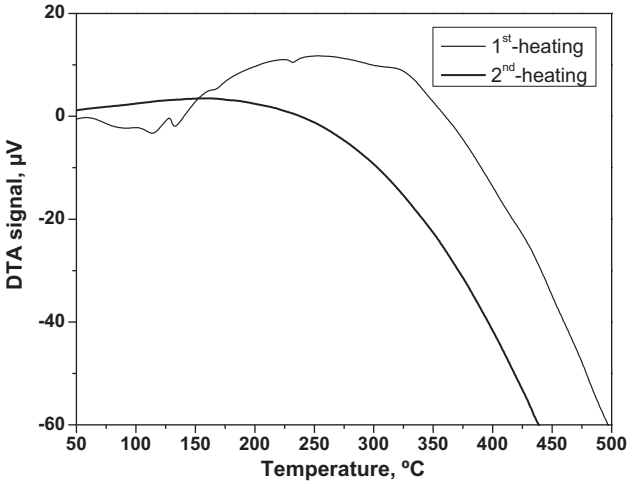

Fig. 4. DTA curves for Fe–Sn–PAN.

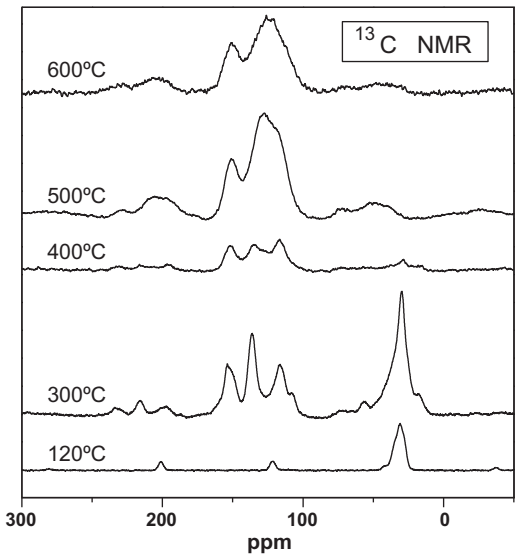

Fig. 5. ^{13}C CP/MAS NMR spectra for PAN dried at 120 °C under vacuum and annealed in inert atmosphere between 300 and 600 °C.

that the thermal treatment of PAN modifies the polymer chains and increases its electrical conductivity [15]. The presence of PAN molecules and the effect of the thermal treatment on the PAN molecules can be observed by using NMR. The ^{13}C CP/MAS NMR spectrum of pristine PAN (Fig. 5) shows a peak at about 30–35 ppm ascribable to sp^3 carbon in the polymer chain (CH and CH_2), another peak at 121 ppm ascribable to unsaturated carbon in C≡N [23,24], and spinning side bands. The treatment of PAN with $NaBH_4$ solution did not modify the ^{13}C NMR spectra (not shown). After heating PAN to 300 °C, the peak at 30 ppm is maintained, the peak at 121 ppm disappears and new peaks emerge. The most intense of these new peaks is located at 135 ppm. Most probably, the peaks at 116 and 135 ppm correspond to the formation of C=C double bonds in the polymer backbone. A peak at 153 ppm can be ascribed to conjugated C=N species [24]. After annealing at 400–600 °C, the peak at 30 ppm disappears and two broadened peaks at observed at 151 and 125 ppm. The ^{13}C CP/MAS NMR spectra of $CoSn_2$@PAN are equivalent to those of pristine PAN (Fig. 6), and this result

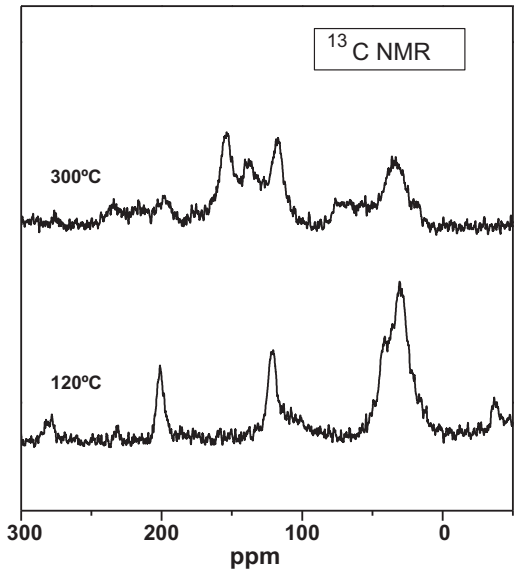

Fig. 6. ^{13}C CP/MAS NMR spectra for $CoSn_2$@PAN dried at 120 °C and annealed in inert atmosphere at 300 °C.

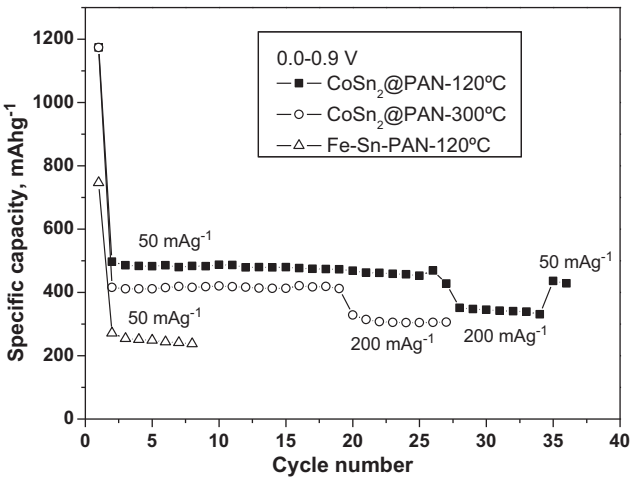

Fig. 7. Specific capacity as a function of cycle number for $CoSn_2$@PAN obtained at 120 and 300 °C, and Fe–Sn–PAN obtained at 120 °C. Initial gravimetric current intensity: 50 mA g^{-1}. Potential window: 0.0–0.9 V. After several cycles, the imposed current was increased to 200 mA g^{-1}.

corroborates the presence of PAN molecules in the $CoSn_2$@PAN sample. The relative intensity of the peak at ca. 30 ppm due to sp^3 carbon indicates that the partial pyrolysis is more extended for $CoSn_2$@PAN-300 °C in comparison with pure PAN heated to 300 °C. It is known that PAN can interact with metallic surfaces and have an easy pyrolysis [15]. From the results of C–N analysis and NMR, it can be concluded that the sample $CoSn_2$@PAN-120 °C contains PAN molecules and $CoSn_2$@PAN-300 °C contains partially pyrolyzed PAN.

The specific capacity is shown in Fig. 7as a function of cycle number. The carbonaceous residua that results from the annealing of PAN at 300 °C can slightly contribute to the capacity [17]. It is worth noting that pure microcrystalline $CoSn_2$ shows high efficiency in the first cycle (85%) but poor capacity retention [1] and that nanocrystalline $FeSn_2$ shows better capacity retention than microstalline $FeSn_2$ [25]. The resulting capacity retention of $CoSn_2$@PAN-120 °C and $CoSn_2$@PAN-300 °C is very good. It is expected that the PAN polymer conforms to the volume changes of the metallic particles that occur during the charge/discharge cycling. PAN is a matrix of structural stability that holds the metallic particle together and allows the migration of the lithium ions. The observed specific capacity of the amorphous $CoSn_2$@PAN-120 °C sample at 50 mA g^{-1} is about 480 mAh g^{-1}. After annealing at 300 °C, the capacity is slightly lower (around 400 mAh g^{-1}), most probably due to the crystallization and grain growth processes and longer lithium ion diffusion path length. A main drawback for the commercial use of these electrode materials would be the high irreversible capacity observed in the first cycle. Hassoun et al. reported an initial irreversible capacity of about 28% for Co–Sn–C alloy [9]. Ionica-Bousquet et al. reported an initial capacity loss for pure $CoSn_2$ of 27% [4]. The $CoSn_2$@PAN electrode shows higher irreverisibility in the first cycle (efficiency of about 43%). The reasons for the observed low initial efficiency can be due to the high reactivity of

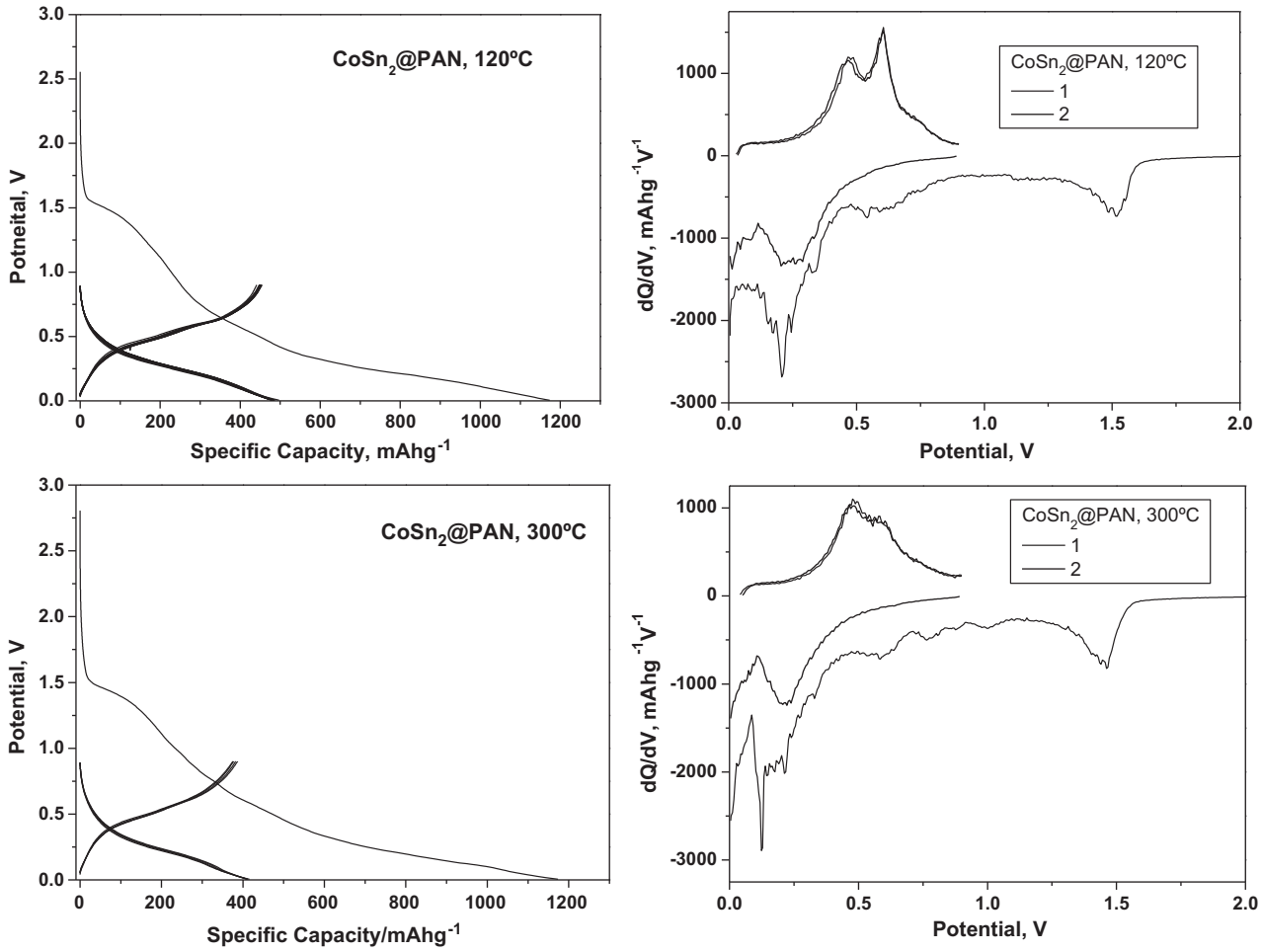

Fig. 8. Potential-capacity curves and differential capacity curves for $CoSn_2$@PAN obtained at 120 and 300 °C. Current intensity: 50 mA g^{-1}. Potential window: 0.0–0.9 V.

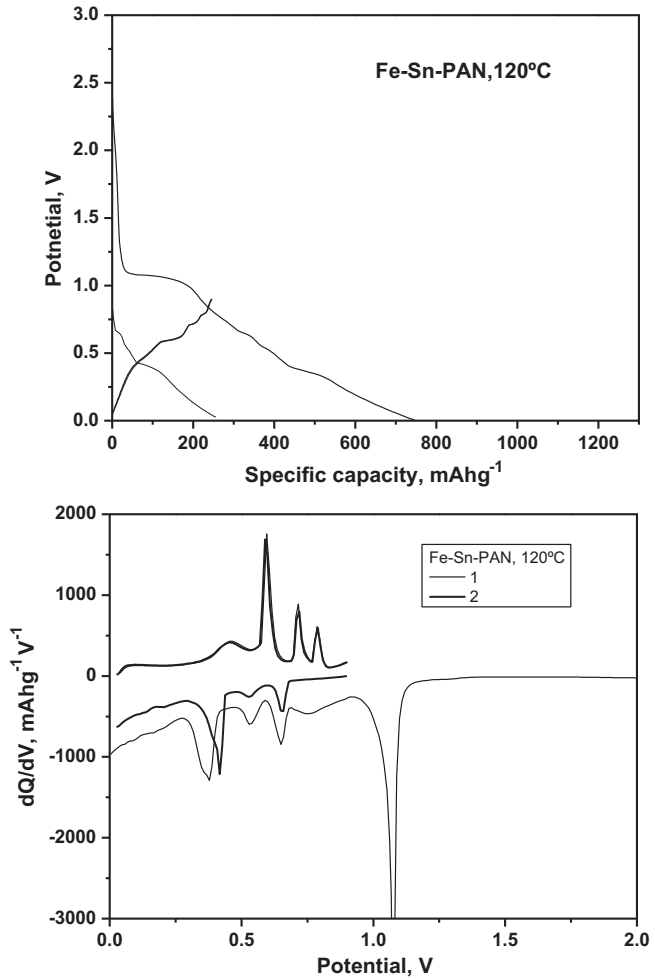

Fig. 9. Potential-capacity curves and derivative plots for Fe–Sn–PAN obtained at 120 °C. Current intensity: 50 mA g^{-1}. Potential window: 0.0–0.9 V.

the surface of the nanoparticles and the low upper potential limit that is imposed. In this context, recently Li et al. found very poor capacity retention and high irreversibility for Co–Sn–C electrodes when PVDF binder is used (60% of capacity loss after 5 cycles), while sodium carboxymethyl cellulose (CMC) binder yields to better electrochemical performance (500 mAh g^{-1} after 90 cycles) [26]. The rate capability of the electrode is another important issue [9]. These PAN-containing materials exhibit a relatively good response to the imposing of higher current intensities, with capacity values of about 350 mAh g^{-1} at 200 mA g^{-1}. The electrochemical behavior of the sample prepared with iron instead of cobalt exhibits poorer electrochemical behavior, as expected due to the presence of crystalline Sn. However, the capacity retention of this electrode material is better than the generally expected for pure Sn.

The galvanostatic cycling results for $CoSn_2$@PAN are shown as potential-capacity plots and derivative curves in Fig. 8. The shape of these derivative curves is rather similar to the cyclic voltammetry reported for Co–Sn–C alloys obtained by mechanical-milling [9]. The derivative plot (d*Q*/d*V* vs. potential) of $CoSn_2$@PAN shows an irreversible peak at 1.5 V in the first discharge that can be ascribed to surface films formation and passivation (solid electrolyte interface). The reaction of lithium with XRD-undetected oxides in the surface of the metallic particles can also contribute to the irreversible capacity of the first discharge. Then, other peaks are observed at ca. 0.6 and 0.2 V. The main peak due to the reaction between Li and pure Sn would occur at 0.4 V [27], but it is not observed. This result suggests the occurrence of a Li–Co–Sn alloy. By definition, the alloy contains metallic grains with different compositions. During the first charge process, a broadened peak is observed with relative maxima at 0.47 and 0.6 V that corresponds to the extraction of lithium from the alloy. The extraction of lithium from crystalline Li_xSn would drive to a narrow peak at 0.8 V in the charge that is not observed here. Additional peaks are observed in the second cycle, at 0.2 V during discharge and 0.47/0.6 V during charge. All these results discard the formation of large and crystalline grains of Li_xSn compounds. These results are in line with a reversible extraction of lithium from an amorphous or poorly crystallized lithium–cobalt–tin alloy. After annealing at 300 °C, the resulting derivative plot exhibits little changes, except a more broadened region in the charge process. The derivative plots of the sample prepared with iron differs from the sample prepared with cobalt. The Fe–Sn–PAN composite electrode shows peaks at 1.1, 0.6, 0.5 and 0.4 V in the first discharge and at 0.5, 0.6, 0.7 and 0.8 V in the first charge (Fig. 9). The irreversible peak at 1.1 V is due to reduction of amorphous oxides and formation of surface films, while the other peaks are ascribed to the reversible formation of Li_xSn phases. Apparently, the iron atoms remain electrochemically inactive.

4. Conclusions

The addition of PAN polymer stabilizes the formation of amorphous Co–Sn alloys throughout reduction of Co(II) and Sn(II) with $NaBH_4$. In contrast, the reduction of Fe(II) and Sn(II) leads to the occurrence of crystalline β-Sn. Amorphous $CoSn_2$@PAN delivers a specific capacity of ca. 480 mAh g^{-1}, which is superior to the maximum capacity of graphite. The PAN molecules stabilize the metallic grains and improve the discharge–charge properties. PAN or pyrolyzed PAN may be a component of future commercial lithium ion batteries based on Co–Sn alloys. However, a major drawback of these electrode materials is the initial irreversible capacity. PAN is studied here because it is a versatile polymer that shows a certain tendency to establish interactions with metallic particles and relatively easy denitrogenation when heated, but other polymers may be used in future works.

Acknowledgements

RA and FN thank the financial support from Ministerio de Ciencia e Innovación (CTQ2008-03192/BQU). JLT acknowledges the financial support from MICNN (MAT2008-05880). The authors are indebted to SCAI-UCO for several instruments facilities.

References

[1] J.J. Zhang, Y.Y. Xia, J. Electrochem. Soc. 153 (2006) A1466.
[2] A.D.W. Todd, R.E. Mar, J.R. Dahn, J. Electrochem. Soc. 154 (2007) A597.
[3] R. Alcántara, I. Rodríguez, J.L. Tirado, ChemPhysChem 9 (2008) 1171.
[4] C.M. Ionica-Bousquet, P.E. Lippens, L. Aldon, J. Olivier-Fourcada, J.C. Jumas, Chem. Mater. 18 (2006) 6442.
[5] R. Alcántara, G. Ortiz, I. Rodríguez, J.L. Tirado, J. Power Sources 189 (2009) 309.
[6] J. Xie, X.B. Zhao, G.S. Cao, J.P. Tu, J. Power Sources 164 (2007) 386.
[7] J.R. Dahn, R.E. Mar, A. Abouzeid, J. Electrochem. Soc. 153 (2006) A361.
[8] R. Alcántara, U. Nwokeke, I. Rodríguez, J.L. Tirado, Electrochem. Solid-State Lett. 11 (2008) A209.
[9] J. Hassoun, S. Panero, G. Mulas, B. Scrosati, J. Power Sources 171 (2007) 928.
[10] Q. Fan, P.J. Chupas, M.S. Whittingham, Electrochem. Solid-State Lett. 10 (2007) A274.
[11] P.P. Ferguson, R.A. Dunlap, J.R. Dahn, J. Electrochem. Soc. 157 (2010) A326.
[12] J.Y. Song, Y.Y. Wang, C.C. Wan, J. Power Sources 77 (1999) 183.
[13] J.F. Snyder, E.L. Wong, C.W. Hubbard, J. Electrochem. Soc. 156 (2009) A215.
[14] Y.J. Kim, H.J. Lee, S.W. Lee, B.W. Cho, C.R. Park, Carbon 43 (2005) 163.
[15] C. Reynaud, C. Boiziau, C. Juret, S. Leroy, J. Perreau, G. Lecayon, Synthetic Metals 11 (1985) 159.
[16] Y. Yu, L. Gu, C.B. Zhu, P.A. van Aken, J. Maier, J. Am. Chem. Soc. 131 (2009) 15894.
[17] F. Nacimiento, R. Alcántara, J.L. Tirado, J. Electrochem. Soc. 157 (2010) A666.
[18] F. Nacimiento, R. Alcántara, J.L. Tirado, J. Alloys Compd. 289 (2009) 135.

[19] L.W. Ji, K.H. Jung, A.J. Medford, X.W. Zhang, J. Mater. Chem. 19 (2009) 4992.
[20] N. Tamura, M. Fujimoto, M. Kamino, S. Fujitani, Electrochim. Acta 49 (2004) 1949.
[21] P. Guilmin, P. Guyot, G. Marchal, Phys. Lett. 109 (1985) 174.
[22] J. Jaén, M.L. Varsányl, E. Kovács, I. Czakó-Nagy, A. Buzás, A. Vértes, L. Kiss, Electrochim. Acta 29 (1984) 1119.
[23] S. Dalton, F. Heatley, P.M. Budd, Polymer 40 (1999) 5531.
[24] S.C. Martin, J.L. Liggat, C.E. Snape, Polym. Degrad. Stabil. 74 (2001) 407.
[25] U.G. Nwokeke, R. Alcántara, J.L. Tirado, R. Stoyanova, M. Yoncheva, E. Zhecheva, Chem. Mater. 22 (2010) 2268.
[26] J. Li, D.B. Le, P.P. Ferguson, J.R. Dahn, Electrochim. Acta 55 (2010) 2991.
[27] F. Nacimiento, R. Alcántara, J.L. Tirado, J. Electroanal. Chem. 642 (2010) 143.